Table S1. Summary of 15 CTMIP5 models with daily meteorology

Model Names [a]	**Resolution**	**Period**	**Country**
BCC-CSM1.1 *	2.81°×2.79°	1850-2100	China
BCC-CSM1.1(M) *	1.125°×1.121°	1850-2100	China
CNRM-CM5 *	1.406°×1.400°	1850-2100	France
CSIRO-Mk3.6.0	1.875°×1.865°	1850-2100	Australia
CanESM2	2.813°×2.789°	1850-2100	Canada
GFDL-CM3	2.500°×2.500°	1860-2100	U.S.
GFDL-ESM2G *	2.500°×2.011°	1861-2100	U.S.
GFDL-ESM2M *	2.500°×2.011°	1861-2100	U.S.
HadGEM2-ES	1.875°×1.250°	1860-2100	U.K.
IPSL-CM5A-LR	3.750°×1.895°	1850-2100	France
IPSL-CM5A-MR	2.500°×1.268°	1850-2100	France
MIROC-ESM-CHEM	2.813°×2.789°	1850-2100	Japan
MIROC-ESM	2.813°×2.789°	1850-2100	Japan
MIROC5 *	1.406°×1.400°	1850-2100	Japan
MRI-CGCM3 *	1.125°×1.121°	1850-2100	Japan

[a] The 7 models denoted by asterisks yield an average temperature below the global warming target of 1.5 °C under the RCP2.6 scenario (Figure S1b). Land carbon simulations driven with meteorology from these 7 models are used for analyses.

Table S2. Summary of 14 TRENDY models for carbon flux evaluations

Model Names [a]	Resolution	Periods	Country
CABLE	0.5°×0.5°	1860-2016	Australia
CLASS-CTEM	2.81°×2.79°	1861-2016	Canada
CLM4.5	1.25°×0.94°	1860-2016	U.S.
DLEM	0.5°×0.5°	1901-2016	U.S.
ISAM	0.5°×0.5°	1860-2016	U.S.
JSBACH	1.88°×1.86°	1860-2016	Germany
JULES	1.88°×1.25°	1860-2016	U.K.
LPJ-wsl	0.5°×0.5°	1901-2016	U.S.
LPX	1.0°×1.0°	1860-2016	Switzerland
OCN	1.0°×1.0°	1860-2016	Germany
ORCHIDEE	0.5°×0.5°	1861-2016	France
ORCHIDEE-MICT	1.0°×1.0°	1860-2016	France
VEGAS	0.5°×0.5°	1860-2016	U.S.
VISIT	0.5°×0.5°	1860-2016	Japan

Table S3. Summary of 12 ACCMIP models with output of O_3 concentrations

Model Names [a]	Resolution	Periods of simulations	Country
CCCma-CMAM	3.75°×3.71°	2011-2020, 2030-2039, 2100-2019	Canada
CICERO-OsloCTM2	2.81°×2.79°	1850, 1910, 1930, 1950, 1970, 1980, 1990, 2000, 2030, 2100	Norway
GFDL-AM3	2.5°×2.0°	1861-1870, 1951-1960, 1981-1990, 2001-2010, 2031-2040, 2051-2060, 2101-2110	U.S.
GISS-E2-R	2.5°×2.0°	1850-2100	U.S.
LLNL-CESM	2.5°×1.89°	1850-1859, 1930-1939, 1980-1989, 2000-2009, 2030-2039, 2100-2109	U.S.
LSCE-LMDzORINCA	3.75°×1.89°	1850-2100	France
MeteoFrance-MOCAGE	2.0°×2.0°	1850-1853, 1930-1933, 1980-1983, 2000-2003, 2030-2033, 2100-2103	France
NCAR-CAM3.5	2.5°×1.89°	1852-1859, 1932-1939, 1982-1989, 2002-2009, 2032-2039, 2102-2109	U.S.
NIES-MIROC-CHEM	2.81°×2.79°	1850-1860, 1930-1934, 1980-1984, 2000-2010, 2030-2034, 2050-2054, 2100-2104	Japan
NIWA-UM-CAM	3.75°×2.5°	1850-1859, 1926-1935, 1976-1985, 1996-2005, 2027-2036, 2090-2099	New Zealand
UEDI-HadAM3	5.0°×5.0°	1851-1860, 1930-1939, 1980-1989, 2000-2009, 2030-2039, 2089-2098	U.K.
UKMO-HadGEM2	1.88°×1.25°	1860-1869, 1980-1989, 2000-2009, 2030-2039, 2100-2109	U.K.

Table S4. Summary of models deriving hourly diffuse radiation

ID	Location	Equation	Reference
M01	China	$k_d = \begin{cases} 0.977 & k_t \leq 0.15 \\ 1.237 - 1.361 \cdot k_t & 0.15 < k_t \leq 0.70 \\ 0.273 & k_t > 0.70 \end{cases}$	Lam and Li (1996)
M02	Canada	$k_d = \begin{cases} 1 - 0.249 \cdot k_t & k_t < 0.35 \\ 1.557 - 1.84 \cdot k_t & 0.35 \leq k_t \leq 0.75 \\ 0.177 & k_t > 0.75 \end{cases}$	Orgill and Hollands (1977)
M03	Europe and U.S.	$k_d = \begin{cases} 1.02 - 0.248 \cdot k_t & k_t \leq 0.30 \\ 1.45 - 1.67 \cdot k_t & 0.3 < k_t < 0.78 \\ 0.147 & k_t \geq 0.78 \end{cases}$	Reindl et al. (1990)
M04	Australia	$k_d = \dfrac{1}{1 + e^{7.997(k_t - 0.586)}}$	Boland et al. (2001)
M05	Singapore	$k_d = \begin{cases} 0.915 & k_t \leq 0.225 \\ 1.135 - 0.9422k_t \\ \quad -0.3878{k_t}^2 & 0.225 < k_t < 0.775 \\ 0.215 & k_t \geq 0.775 \end{cases}$	Hawlader (1984)
M06	Europe	$k_d = \begin{cases} 0.995 - 0.081k_t & k_t \leq 0.21 \\ 0.724 + 2.738k_t \\ \quad -8.32{k_t}^2 + 4.967{k_t}^3 & 0.21 < k_t \leq 0.76 \\ 0.18 & k_t > 0.76 \end{cases}$	De Miguel et al. (2001)
M07	Greece	$k_d = \begin{cases} 0.9995 - 0.05k_t \\ \quad -2.4156{k_t}^2 + 1.4926{k_t}^3 & 0 < k_t \leq 0.78 \\ 0.20 & k_t > 0.78 \end{cases}$	Karatasou et al. (2003)
M08	U.S.	$k_d = \begin{cases} 1.0 - 0.09k_t & k_t \leq 0.22 \\ 0.951 - 0.1604k_t \\ \quad +4.388{k_t}^2 - 16.638{k_t}^3 \\ \quad +12.336{k_t}^4 & 0.22 < k_t \leq 0.80 \\ 0.165 & k_t > 0.80 \end{cases}$	Erbs et al. (1982)
M09	India	$k_d = \begin{cases} 1.0086 - 0.178k_t & k_t \leq 0.24 \\ 0.9686 + 0.1325k_t \\ \quad +1.4183{k_t}^2 - 10.1862{k_t}^3 \\ \quad +8.3733{k_t}^4 & 0.24 < k_t \leq 0.80 \\ 0.197 & k_t > 0.80 \end{cases}$	Chandrasekaran and Kumar (1994)
M10	Brazil	$k_d = \begin{cases} 1.0 & k_t \leq 0.17 \\ 0.97 + 0.8k_t - 3.0{k_t}^2 \\ \quad -3.1{k_t}^3 + 5.2{k_t}^4 & 0.17 < k_t \leq 0.75 \\ 0.17 & k_t > 0.75 \end{cases}$	Oliveira et al. (2002)
M11	Brazil	$k_d = \begin{cases} 1.0 & k_t \leq 0.17 \\ 0.9 + 1.1k_t - 4.5{k_t}^2 \\ \quad +0.01{k_t}^3 + 3.14{k_t}^4 & 0.17 < k_t \leq 0.75 \\ 0.17 & k_t > 0.75 \end{cases}$	Soares et al. (2004)

Table S5. Measurements of O_3 effects to plant photosynthesis in China

PFT[a]	Species	O_3 (ppbv)	Change (%) Mean	Max	Min	Study
DBF	*Acer truncatum Bunge*	106	-7.2	-9.3	-4.3	Li et al. (2015)
		134	-30.2	-38.1	-19.8	
	Ailanthus altissima	69	-17	-17	-17	Hoshika et al. (2014)
		100	-28.1	-28.1	-28.1	
	Fraxinus chinensis	69	-27.9	-27.9	-27.9	
		100	-43.2	-43.2	-43.2	
	Platanus orientalis	69	-0.9	-0.9	-0.9	
		100	-35.2	-35.2	-35.2	
	Betula platyphylla	160	-50.9	-50.9	-50.9	Fu et al. (2014)
	Populus alba×P. Berolinensi	160	-24.4	-24.4	-24.4	
	Ginkgo biloba	80	-21	-53	-5	He et al. (2007)
		80	-21.9	-34.1	2.10	Zhang et al. (2007a)
		85	-8.8	-35.5	16.2	Xu et al. (2015)
	liriodendron chinense	80	-29.7	-41	-22.3	Zhang et al. (2011c)
		150	-42	-44	-40	Zhang et al. (2012)
	Liquidambar formosana	150	-36	-41	-30	
	Metasequoia glyptostroboides	50	0	0	0	Feng et al. (2008a)
		100	-40.9	-40.9	-40.9	
		200	-49.7	-49.7	-49.7	
		54	-20.6	-31.5	-14.7	Zhang et al. (2014)
	Populus 111	58	-12.7	-12.7	-12.7	Xin et al. (2016)
		74	-36.8	-36.8	-36.8	
		87	-49.8	-49.8	-49.8	
		108	-59.1	-59.1	-59.1	
		124	-72	-72	-72	
	Populus 546	58	-7.8	-7.8	-7.8	
		73	-30.1	-30.1	-30.1	
		86	-36.6	-36.6	-36.6	
		106	-47	-47	-47	
		122	-74.5	-74.5	-74.5	
	Populus wq	58	-3.1	-3.1	-3.1	
		74	-19.8	-19.8	-19.8	
		87	-44.6	-44.6	-44.6	
		108	-51.4	-51.4	-51.4	
		124	-69.2	-69.2	-69.2	
	Quercus mongolica	80	-50.7	-54.8	-48.4	Yan et al. (2010)
		80	-55.7	-73.3	-35.7	Wang et al. (2009)
		85	-38.9	-63.7	-1.3	Xu et al. (2015)
ENF	*Pinus tabulaeformis*	80	-23.7	-47.3	10.7	Zhang et al. (2007b)
		80	-27.6	-45	-9.4	Zhao et al. (2009)
		85	-35.4	-39.8	-31.2	Xu et al. (2014)
		85	-30.8	-46.3	-16	Xu et al. (2015)
	Pinus armandii	85	-37.6	-59.3	-9.1	
	Pinus elliottii	80	-42.7	-42.7	-42.7	Zhang et al. (2011b)

EBF	*Alstonia scholaris*	150	-1.1	-6.4	4.5	Hao et al. (2014)
	Syzygium hainanense	150	-17.3	-17.4	-17.1	
	Cinnamomum camphora	95	-28	-32	-20	Feng et al. (2011a)
		58	-12.4	-19.1	-5.3	Niu et al. (2014)
		88	-24.1	-32.6	-12.1	
		150	-27	-36	-13	Zhang et al. (2012)
	Cyclobalanopsis glauca	150	-29	-33	-24	
	Neolitsea sericea	150	-16	-29	-4	
	Schima superba	150	-32	-49	-19	
	Castanopsis fissa	150	-47.9	-47.9	-47.8	Li et al. (2014)
	Elaeocarpus apiculatus	150	-28	-31.1	-24.6	
	Mytilaria laosensis	150	-19.3	-30	-8.6	
	Ilex integra Thunb	150	-9.6	-19.1	-4	Zhang et al. (2011a)
	Lindera setchuenensis	80	-27.9	-39.2	-17.9	Li (2015)
		140	-14.3	-28	-3.2	
		200	-45.5	-61.8	-32.7	
	Machilus pauhoi	80	-24.3	-51.6	3.5	
		140	-18.9	-39.6	24.4	
		200	-23.9	-33.3	5.5	
	Machilus thunbergii	80	10.6	-5.2	21.1	
		140	12.9	5.6	17.4	
		200	-7.9	-39.2	16.7	
	Ohoebe chekiangensis	80	-19.7	-52.5	15.2	
		140	-45.9	-112.4	-8.8	
		200	-33.1	-84	13.6	
	Phoebe bournei	80	10.4	-10.7	22.9	
		140	2.2	-8.2	15.6	
		200	-29.1	-44.1	-11.3	
	Phyllostachys edulis	97	-47.6	-80.6	-12.1	Zhuang et al. (2013)
C4	Maize	80	-23.5	-33.7	-16.8	Fu et al. (2008)
Crop	Rice	54	-15.6	-22.7	-8.4	Pang et al. (2009)
	Snap bean	71	-22	-38.8	-4.5	Yuan et al. (2015)
	Wheat	82	-24	-35	-12	Biswas et al. (2008)
		82	-21.1	-28	-13.3	Biswas et al. (2009)
		73	-20	-24	-20	Feng et al. (2008b)
		55	-12.9	-18.4	-7.3	Feng et al. (2011b)
		100	-18.3	-38.2	-8.2	Zheng et al. (2010)
		150	-25.9	-42.5	-5.8	

[a] Plant functional types (PFTs), including deciduous broadleaf forest (DBF), evergreen needleleaf forest (ENF), evergreen broadleaf forest (EBF), C4 and C3 crops.

Table S6. YIBs simulations with CMIP5 meteorology

Group simulations [a]	Scenario	CO_2	TAS	QAS	SOILM	RAD
RCP26_ALL	RCP2.6	2001-2100	2001-2100	2001-2100	2001-2100	2001-2100
RCP26_CO2	RCP2.6	2001-2100	2000	2000	2000	2000
RCP26_MET	RCP2.6	2000	2001-2100	2001-2100	2001-2100	2001-2100
RCP26_TAS	RCP2.6	2000	2001-2100	2000	2000	2000
RCP26_QAS	RCP2.6	2000	2000	2001-2100	2000	2000
RCP26_SOL	RCP2.6	2000	2000	2000	2001-2100	2000
RCP26_RAD	RCP2.6	2000	2000	2000	2000	2001-2100
RCP85_ALL	RCP8.5	2001-2100	2001-2100	2001-2100	2001-2100	2001-2100
RCP85_CO2	RCP8.5	2001-2100	2000	2000	2000	2000
RCP85_MET	RCP8.5	2000	2001-2100	2001-2100	2001-2100	2001-2100
RCP85_TAS	RCP8.5	2000	2001-2100	2000	2000	2000
RCP85_QAS	RCP8.5	2000	2000	2001-2100	2000	2000
RCP85_SOL	RCP8.5	2000	2000	2000	2001-2100	2000
RCP85_RAD	RCP8.5	2000	2000	2000	2000	2001-2100
HIST_2000	HIST	2000	2000	2000	2000	2000

[a] Each group includes 7 YIBs runs driven with meteorology from different CMIP5 models, making a total of 105 simulations. All simulations are performed for period of 1850-2100 with the first 10 years of spin up. For the same climate model, all groups share the same historical meteorology from 1850 to 2000. After the year 2000, different groups use climate forcing fixed at the year 2000 for certain variables.

Table S7. YIBs simulations for ozone damaging effects

Group simulations [a]	Scenario	O_3	Damaging sensitivity
RCP26_O3H	RCP2.6	1850-2100	High
RCP26_O3L	RCP2.6	1850-2100	Low
RCP85_O3H	RCP8.5	1850-2100	High
RCP85_O3L	RCP8.5	1850-2100	Low

[a] Each group includes 7 YIBs runs driven with meteorology from different CMIP5 models, making a total of 28 simulations. All simulations are performed for period of 1850-2100 with the first 10 years of spin up. For the same climate model, all groups share the same historical meteorology from 1850 to 2000. After the year 2000, different groups use different future scenarios (RCP2.6 or RCP8.5). To predict O_3-induced GPP loss, the YIBs model is driven with ensemble average O_3 concentrations simulated with 12 ACCMIP models (Table S3) for different scenarios (RCP2.6 or RCP8.5) or different damaging sensitivities (high or low).

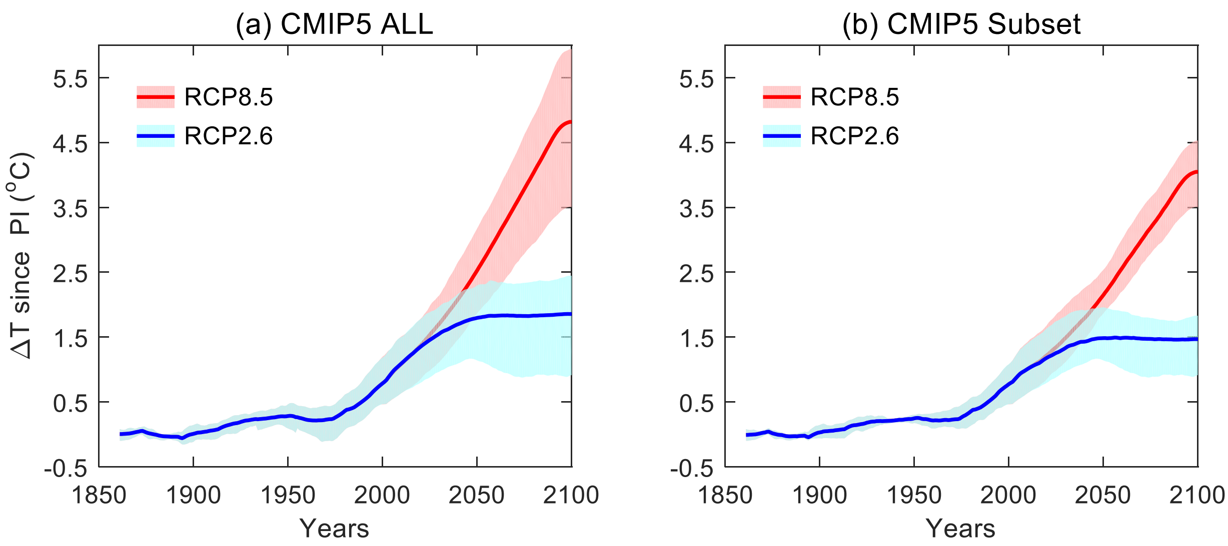

Figure S1. Changes in global temperature since preindustrial (PI). Global average temperature under RCP2.6 (blue) and RCP8.5 (red) scenarios from CMIP5 models are calculated and smoothed with 21-year window. Mean temperature for 1861-1900 is subtracted from global time series to derive temperature anomalies since PI. The bold lines are model ensemble mean values with shading of uncertainties for CMIP5 simulations. Results for all available models (15 in total) providing required daily meteorology are shown in the left, and those for the subset of models (7 in total) yielding equilibrium temperature below 1.85ºC for 2060-2100 are shown in the right.

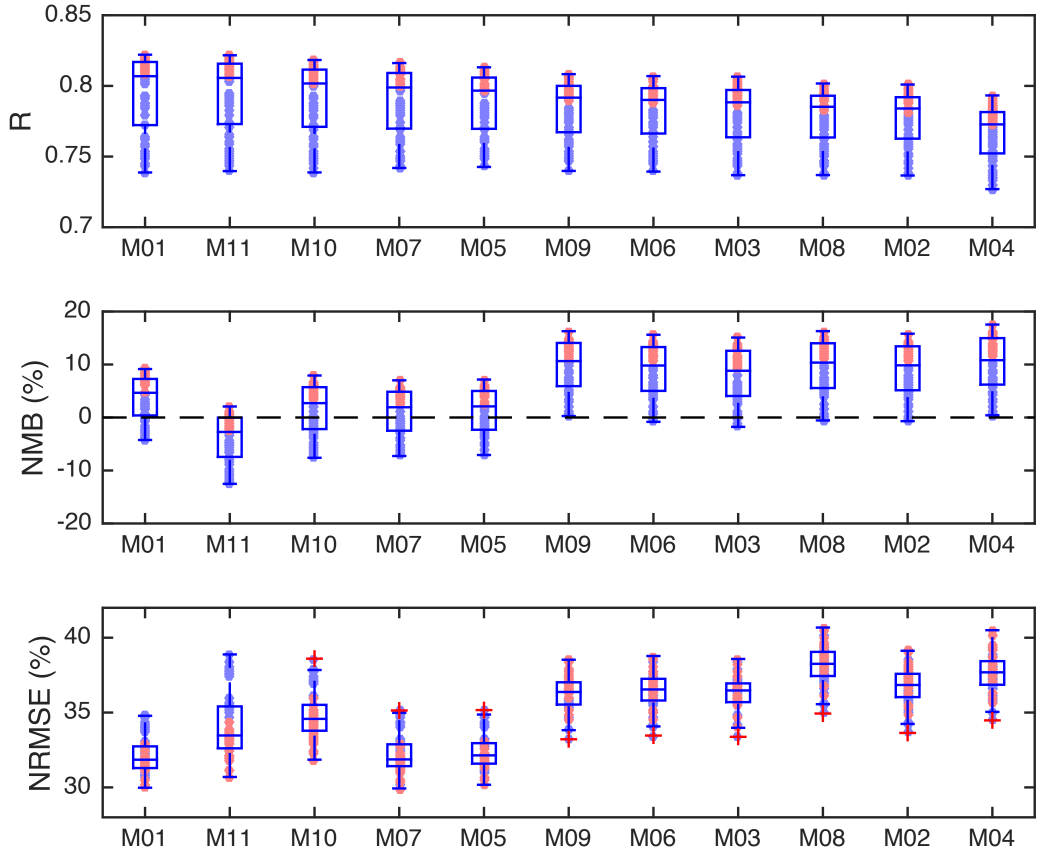

Figure S2. Inter-comparison of 11 methods deriving diffuse radiation. Results shown are statistical metrics for derived and original diffuse radiation from MERRA reanalysis over China. The statistical metrics include correlation coefficient (R), normalized mean biases (NMB), and normalized root mean square error (NRMSE). Each dot represents one out of 60 months for the validation period of 2008-2012, with red indicating growth season (May-September) and blue for other months. Each symbol on x axis represents a method listed in Table S4, which is used to calculate diffuse radiation from total radiation at hourly time step.

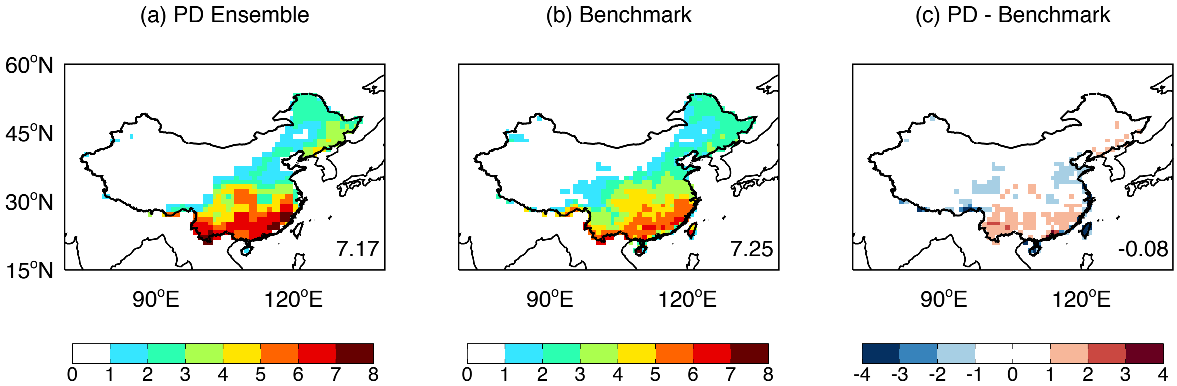

Figure S3. Evaluation of simulated GPP for present day. Results shown are annual GPP from (a) ensemble mean of simulations, (b) benchmark product, and (c) their differences for the period of 1982-2011. The simulations are performed using YIBs vegetation model driven with historical meteorology from 7 selected CMIP5 models. The benchmark product is upscaled from available FLUXNET sites using an ensemble of regression trees (Jung et al., 2009). The total values (Pg C yr^{-1}) over China are shown in each panel. Units of colorbar: g C m^{-2} day^{-1}.

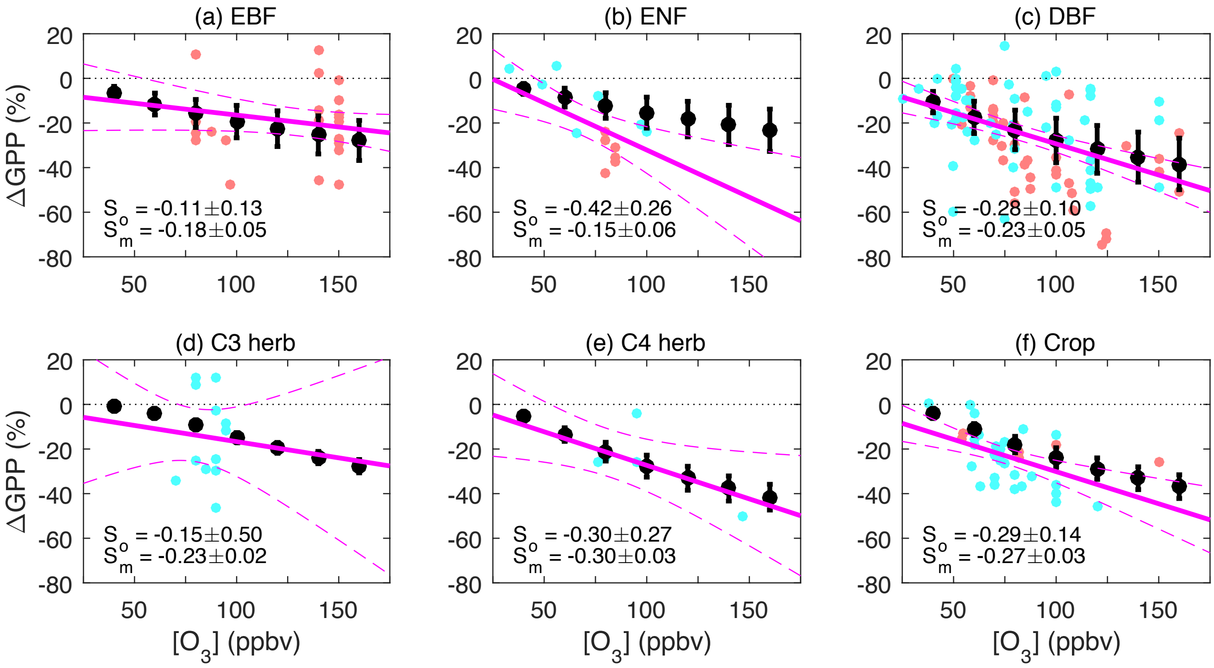

Figure S4. Evaluation of O_3 damaging effects to photosynthesis with literature meta-analysis. Results shown are the percentage changes in GPP for six main plant functional types (PFTs). Points on each panel represent results summarized from literature with red for China (Table S5) and blue for global (Yue and Unger, 2018). The linear regression is denoted as a red solid line, with 95% confidence intervals shown as dashed lines. Black points represent simulated GPP sensitivity to different level of O_3 in China, with error bars indicating the range of prediction from low to high O_3 damaging sensitivities. The slopes of observed (S_o, mean ± 95% confidence interval) and modeled (S_m, mean ± (high-low)/2 sensitivity) GPP-O_3 sensitivity is shown on each panel.

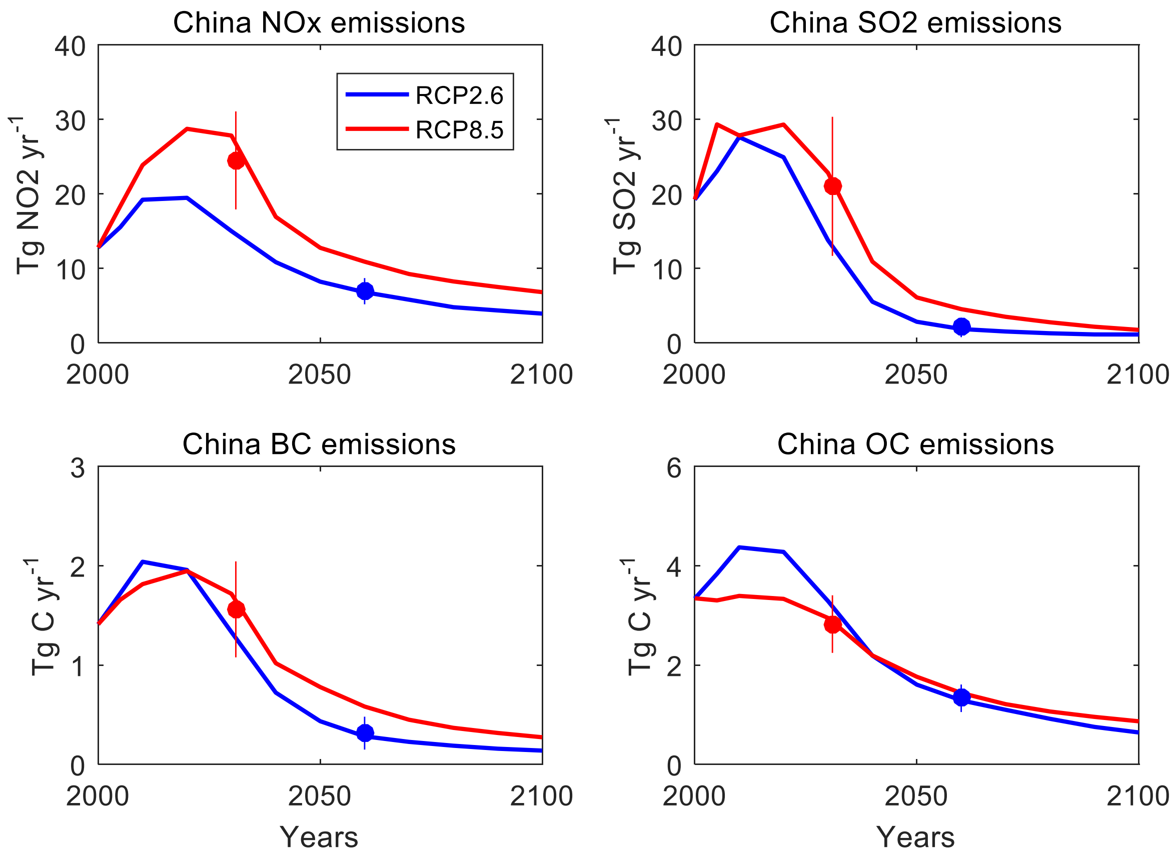

Figure S5. Changes in anthropogenic emissions in China for two RCP scenarios. Results shown are the total emissions of NO_x, SO_2, black carbon (BC), and organic carbon (OC) over China during 2010-2100 for RCP2.6 (blue) and RCP8.5 (red) scenarios. The average country-level emissions for the period of the global warming of 1.5°C are shown as blue points for RCP2.6 scenario (2050-2070) and red points for RCP8.5 scenario (2021-2041). Error bars indicate one standard deviation of emissions during the specific periods.

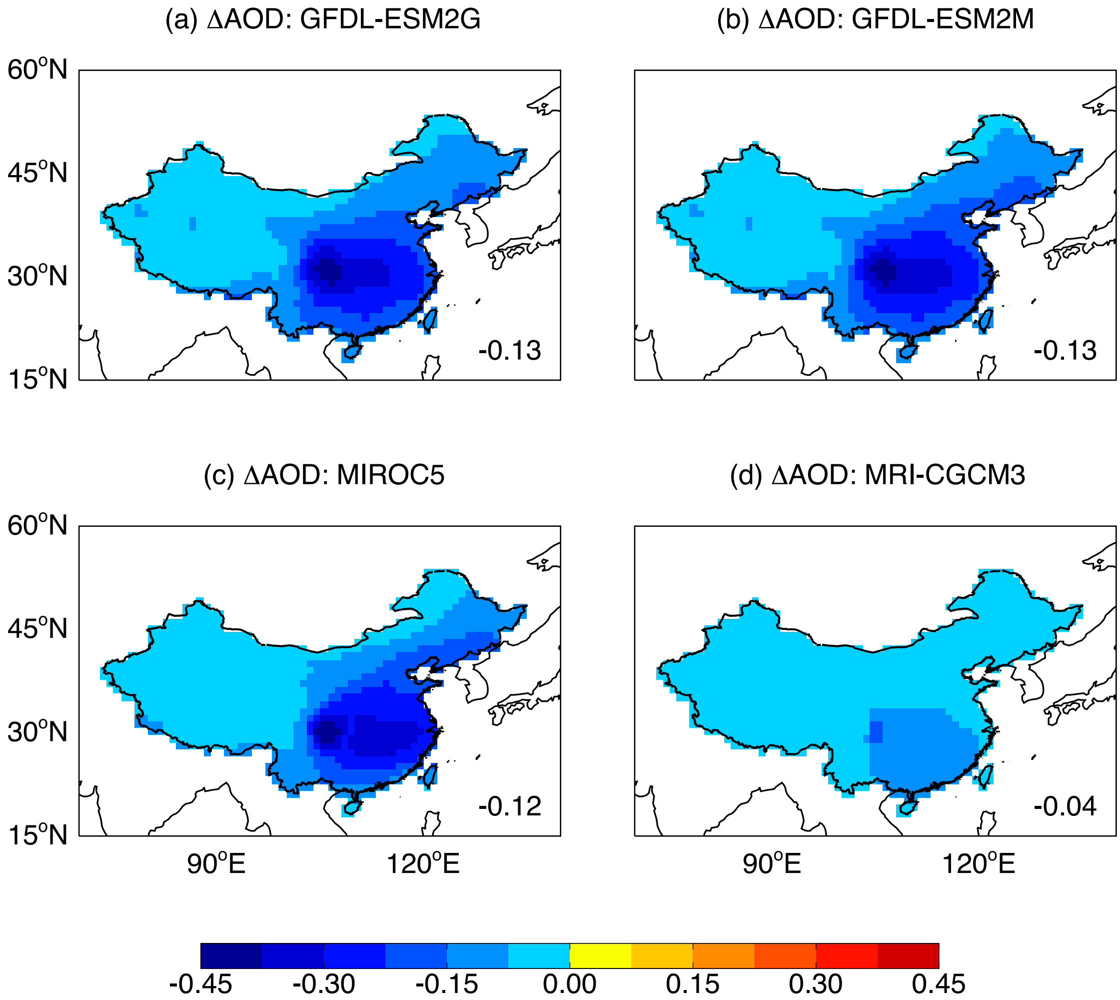

Figure S6. Differences in aerosol optical depth (AOD) in China for two RCP scenarios. Results shown are the differences of AOD at 550 nm for the global warming of 1.5°C between RCP2.6 scenario (2050-2070) and RCP8.5 scenario (2021-2041). Only 4 out of 7 selected models, including GFDL-ESM2G, GFDL-ESM2M, MIROC5, and MRI-CGCM3, provide archived output of AOD at both scenarios. The mean differences over China are shown in each panel.

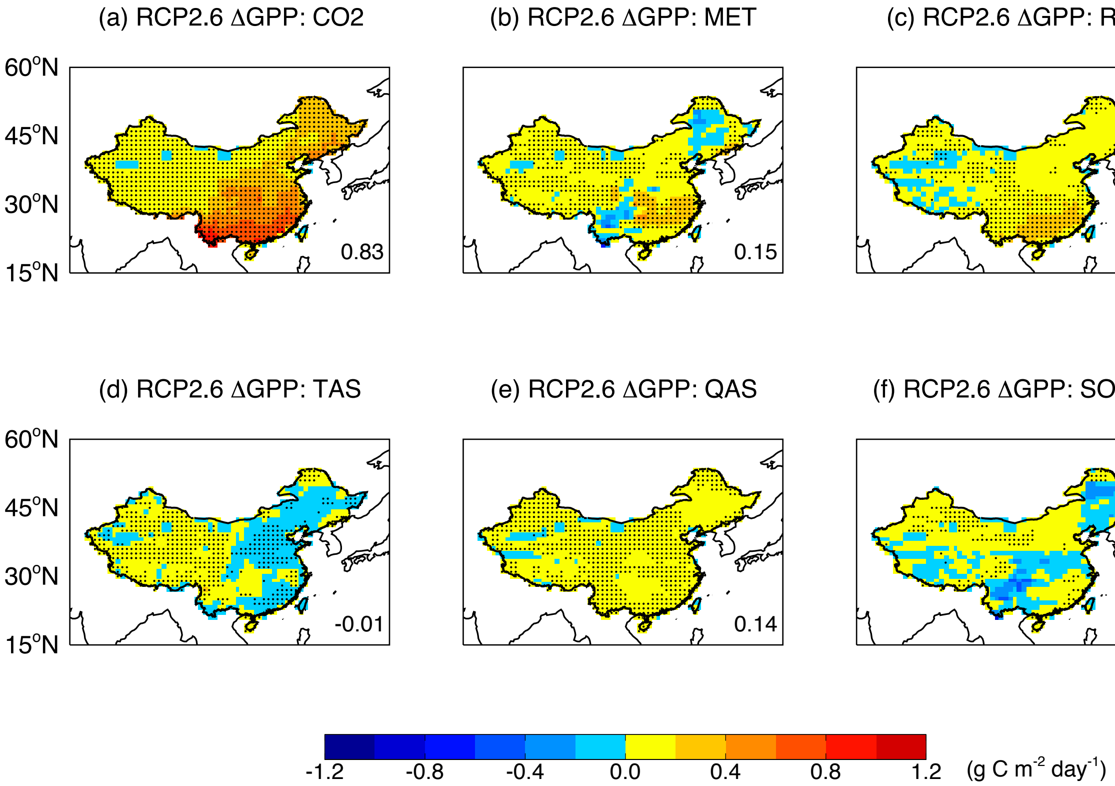

Figure S7. Changes in gross primary production (GPP) caused by individual driving factors. Results shown are changes in GPP between the period of global warming of 1.5ºC (2050-2070) and present day (1995-2015) caused by variations in selected drivers for the RCP2.6 scenario. Before the year 2000, historical meteorology and CO_2 concentrations are applied for each simulation. After the year 2000, all forcings are fixed at the level of the year 2000, except for (a) CO_2 concentrations, (b) all meteorology, (c) shortwave radiation, (d) temperature, (e) specific air humidity, and (f) soil moisture. For each grid, significant changes at p<0.05 are marked with dots. The total changes (Pg C yr^{-1}) over China are shown in each panel.

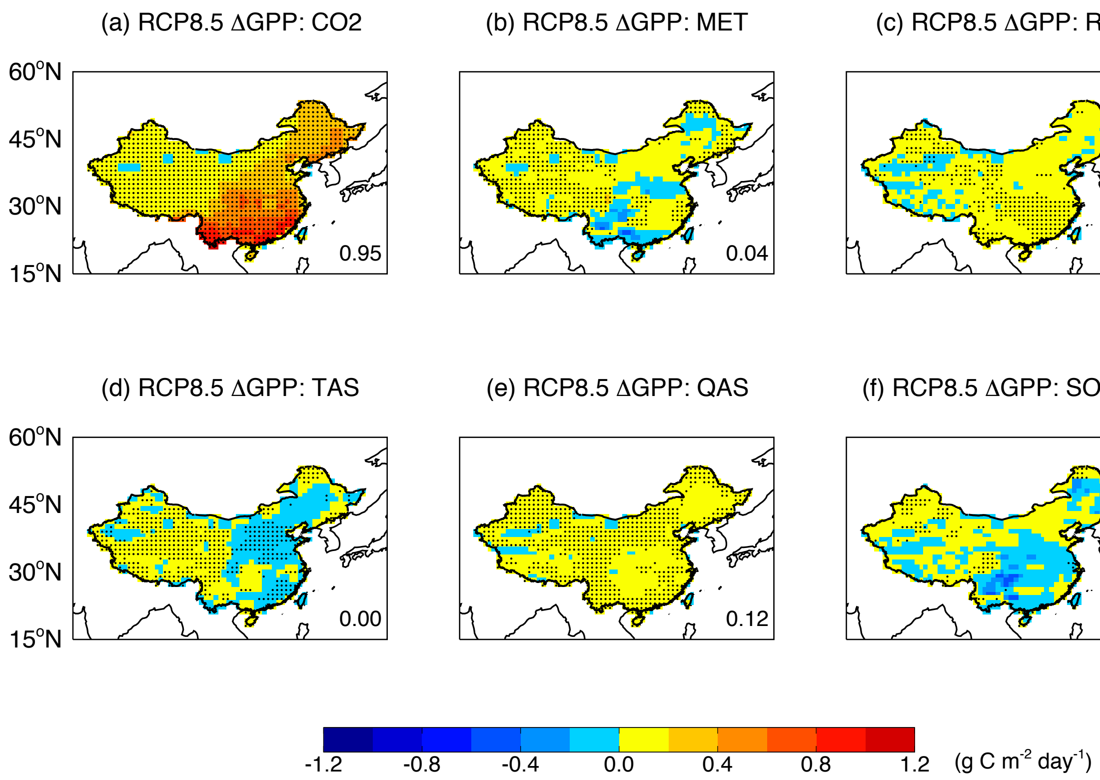

Figure S8. The same as Figure S7 except for RCP8.5 scenario. The period of global warming of 1.5ºC is 2021-2041 for the RCP8.5 scenario.

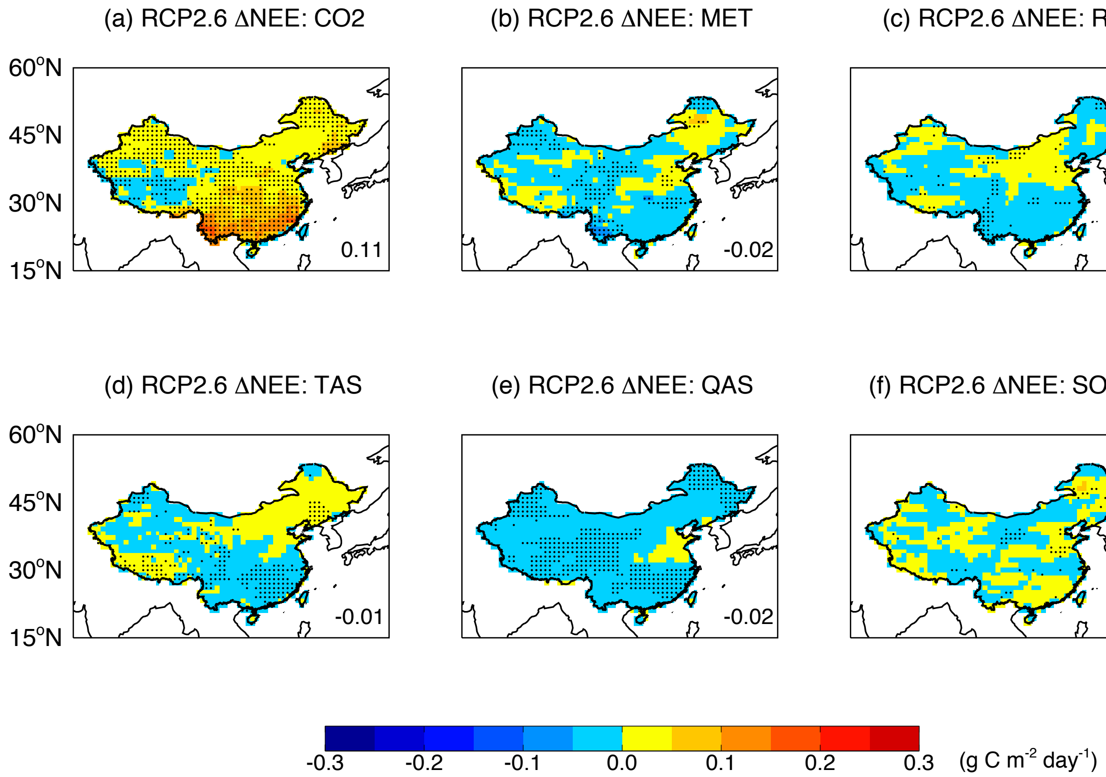

Figure S9. Changes in net ecosystem exchange (NEE) caused by individual driving factors. Results shown are changes in NEE between the period of global warming of 1.5ºC (2050-2070) and present day (1995-2015) caused by variations in selected drivers for the RCP2.6 scenario. Before the year 2000, historical meteorology and CO_2 concentrations are applied for each simulation. After the year 2000, all forcings are fixed at the level of the year 2000, except for (a) CO_2 concentrations, (b) all meteorology, (c) shortwave radiation, (d) temperature, (e) specific air humidity, and (f) soil moisture. For each grid, significant changes at $p<0.05$ are marked with dots. The total changes (Pg C yr^{-1}) over China are shown in each panel.

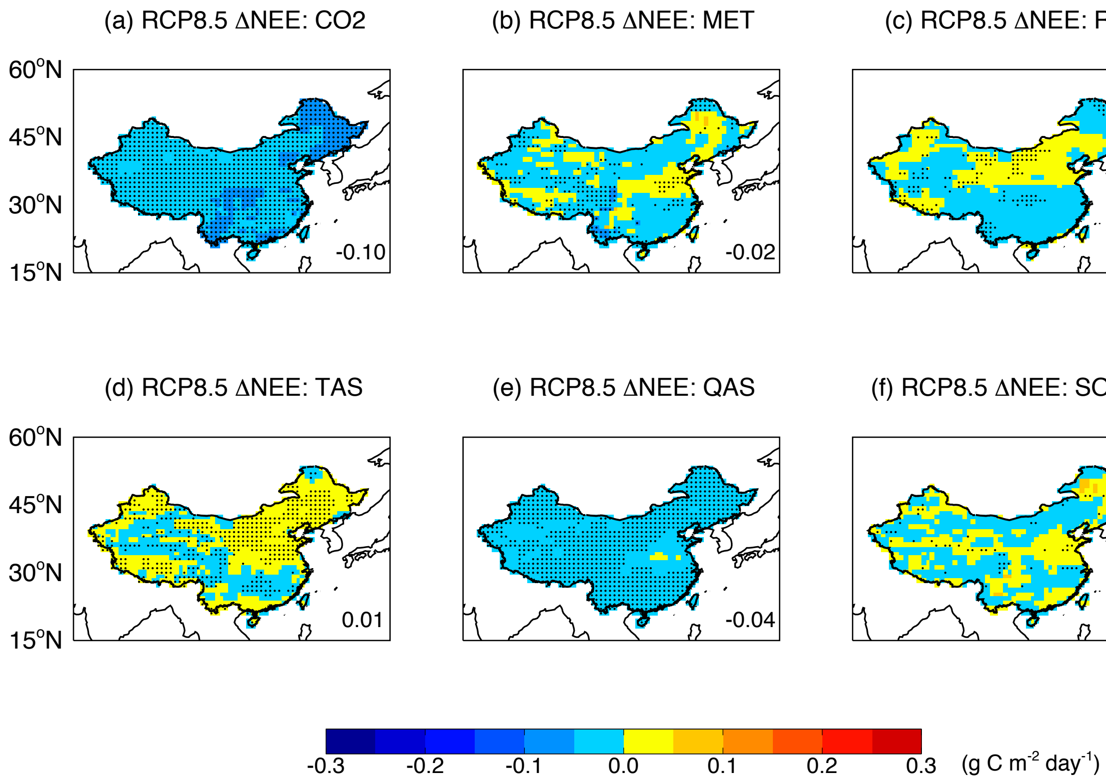

Figure S10. The same as Figure S9 except for RCP8.5 scenario. The period of global warming of 1.5ºC is 2021-2041 for the RCP8.5 scenario.

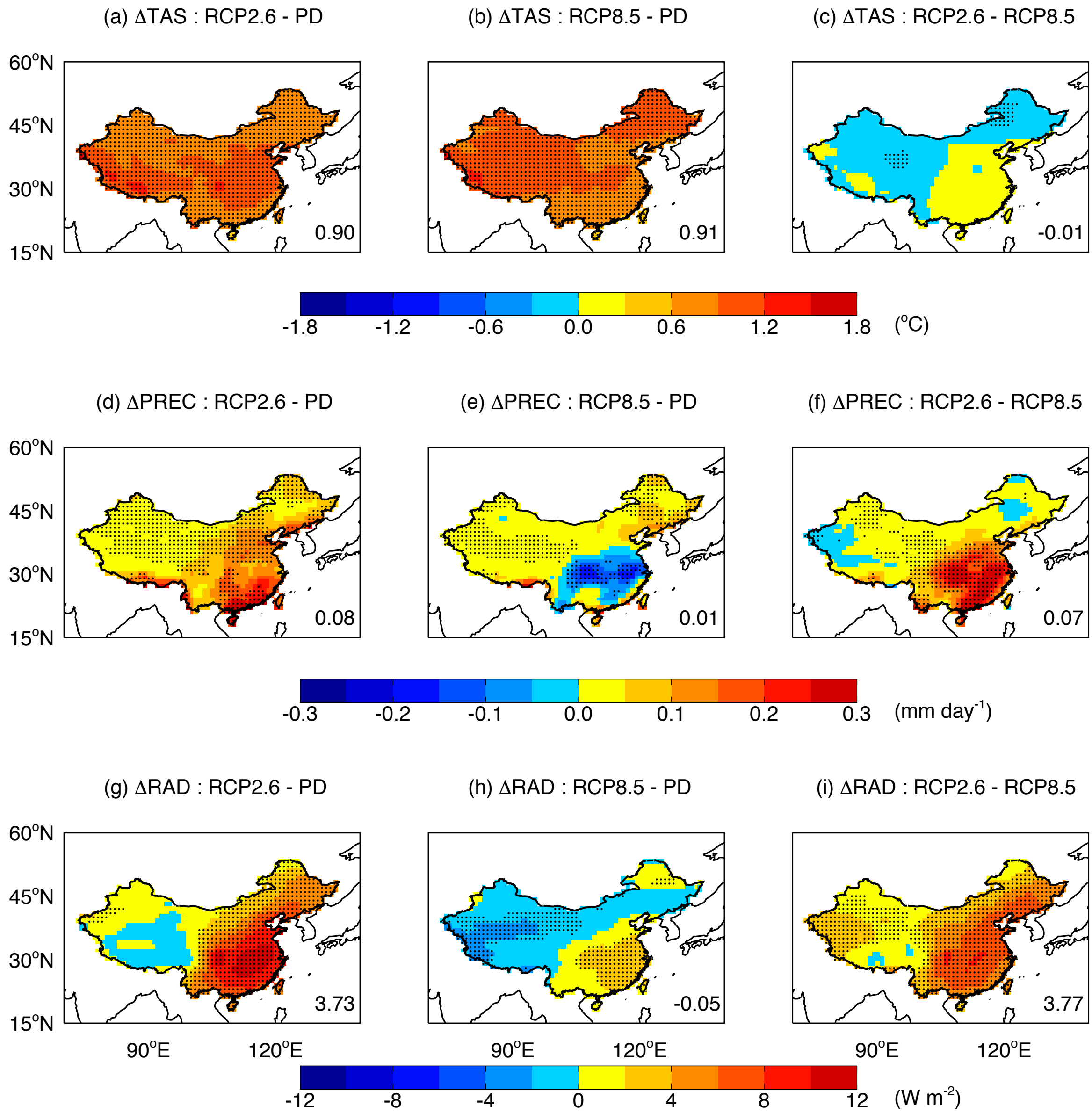

Figure S11. Projected changes in meteorology for two RCP scenarios. Results shown are simulated (top) surface air temperature, (middle) precipitation, and (bottom) surface downward shortwave radiation over China between the period of global warming of 1.5°C and present day (1995-2015) under (left) RCP2.6 scenario (2050-2070), (middle) RCP8.5 scenario (2021-2041), and (right) their differences. Analyses are based on meteorology from 7 CMIP5 models. For each grid, significant changes at $p<0.05$ are marked with dots. The mean changes over China are shown in each panel.

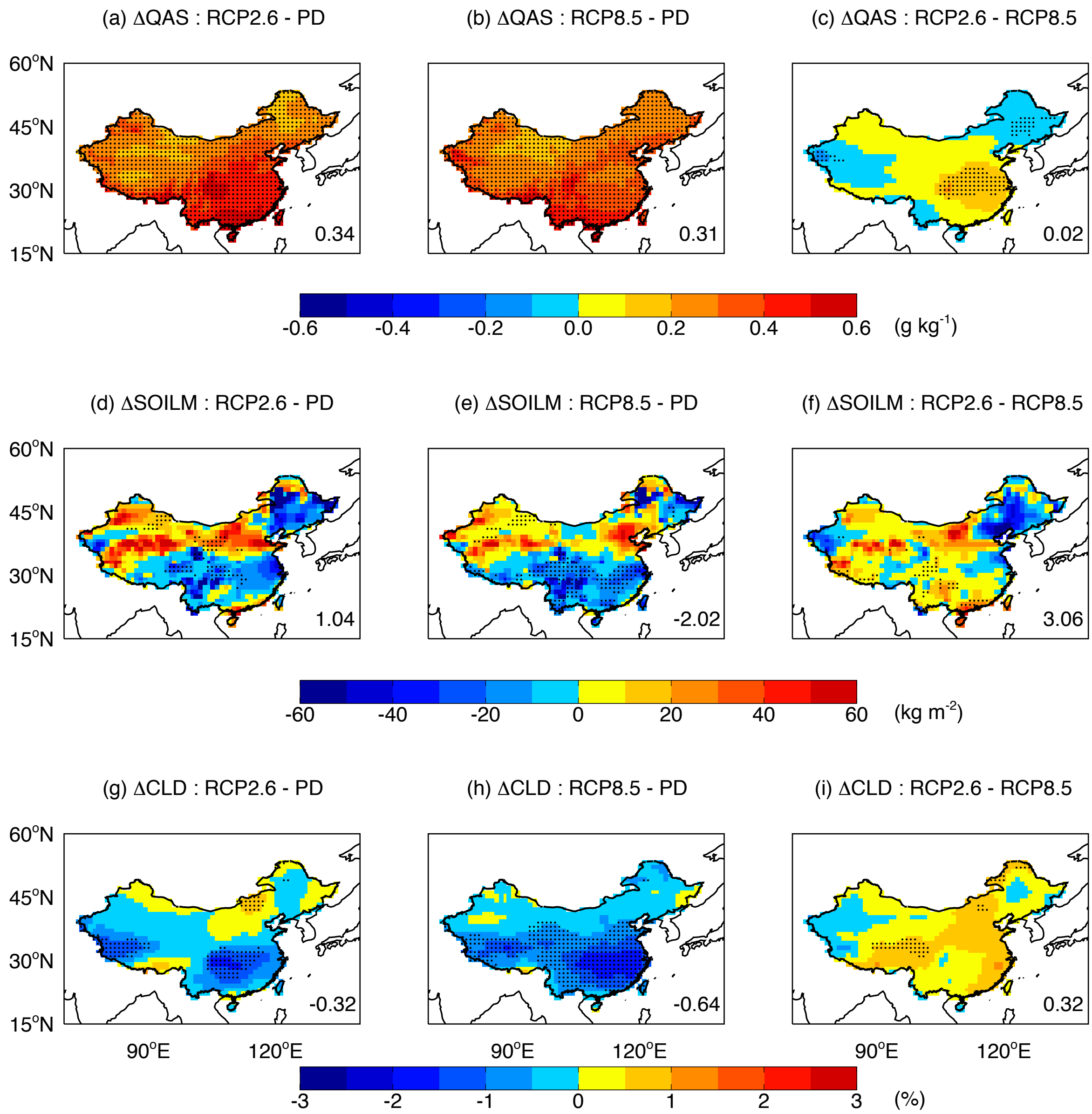

Figure S12. The same as Figure S11 but for changes in (top) surface air humidity, (middle) soil moisture content, and (bottom) cloud amount.

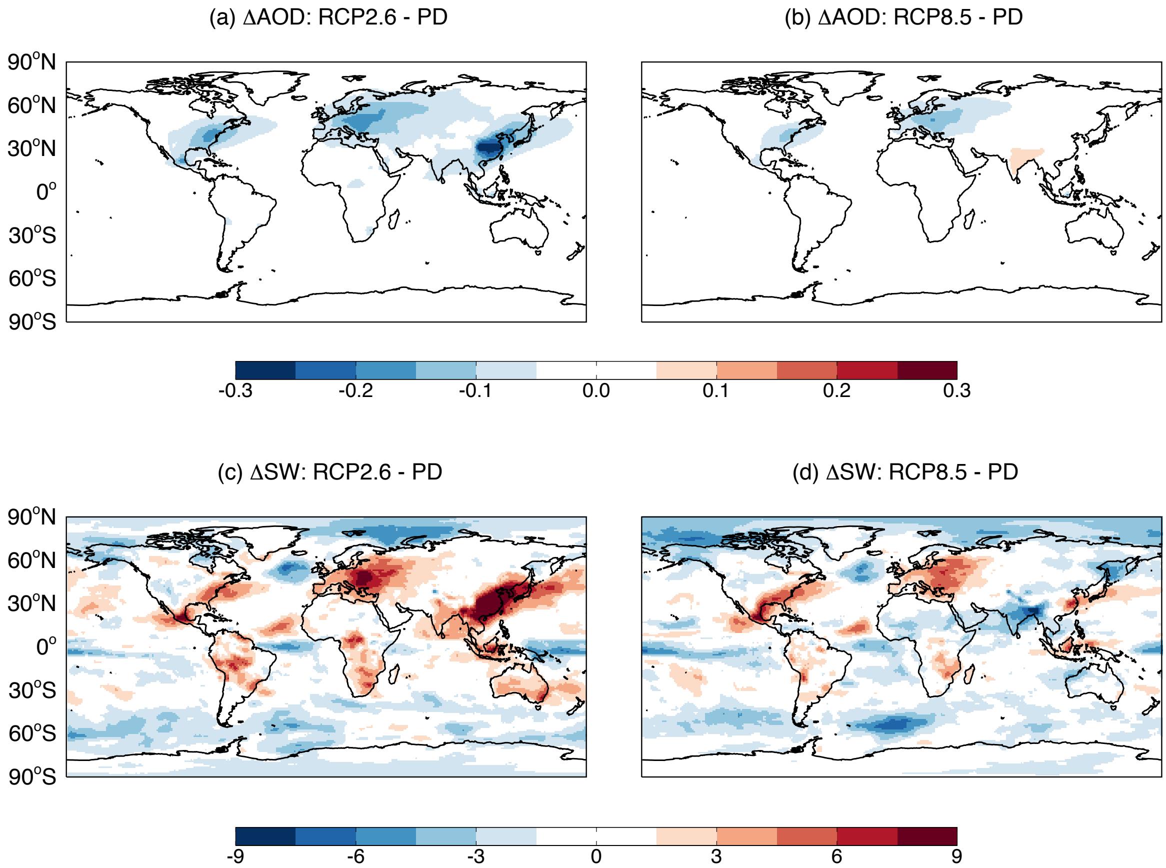

Figure S13. Projected changes in AOD and shortwave radiation for two RCP scenarios. Global changes are shown for (a, b) AOD and (c, d) surface downward shortwave radiation (W m^{-2}) between the period of global warming of 1.5ºC and present day (1995-2015) under (left) RCP2.6 (2050-2070) and (right) RCP8.5 scenario (2021-2041). Analyses are the ensemble average of GFDL-ESM2G, GFDL-ESM2M, MIROC5, and MRI-CGCM3, which provide archived output of AOD at both RCP2.6 and RCP8.5 scenarios.

References

Biswas, D. K., Xu, H., Li, Y. G., Sun, J. Z., Wang, X. Z., Han, X. G., and Jiang, G. M.: Genotypic differences in leaf biochemical, physiological and growth responses to ozone in 20 winter wheat cultivars released over the past 60 years, Global Change Biology, 14, 46-59, doi:10.1111/j.1365-2486.2007.01477.x, 2008.

Biswas, D. K., Xu, H., Yang, J. C., Li, Y. G., Chen, S. B., Jiang, C. D., Li, W. D., Ma, K. P., Adhikary, S. K., Wang, X. Z., and Jiang, G. M.: Impacts of methods and sites of plant breeding on ozone sensitivity in winter wheat cultivars, Agriculture Ecosystems & Environment, 134, 168-177, doi:10.1016/j.agee.2009.06.009, 2009.

Boland, J., Scott, L., and Luther, M.: Modelling the diffuse fraction of global solar radiation on a horizontal surface, Environmetrics, 12, 103-116, doi:10.1002/1099-095x(200103)12:2<103::Aid-Env447>3.0.Co;2-2, 2001.

Chandrasekaran, J., and Kumar, S.: Hourly Diffuse Fraction Correlation at a Tropical Location, Sol Energy, 53, 505-510, doi:10.1016/0038-092x(94)90130-T, 1994.

De Miguel, A., Bilbao, J., Aguiar, R., Kambezidis, H., and Negro, E.: Diffuse solar irradiation model evaluation in the North Mediterranean belt area, Sol Energy, 70, 143-153, doi:10.1016/S0038-092x(00)00135-3, 2001.

Erbs, D. G., Klein, S. A., and Duffie, J. A.: Estimation of the Diffuse-Radiation Fraction for Hourly, Daily and Monthly-Average Global Radiation, Sol Energy, 28, 293-302, doi:10.1016/0038-092x(82)90302-4, 1982.

Feng, Z., Zeng, H., Wang, X., Zheng, Q., and Feng, Z.: Sensitivity of Metasequoia glyptostroboides to ozone stress, Photosynthetica, 46, 463-465, 2008a.

Feng, Z. Z., Kobayashi, K., and Ainsworth, E. A.: Impact of elevated ozone concentration on growth, physiology, and yield of wheat (Triticum aestivum L.): a meta-analysis, Global Change Biology, 14, 2696-2708, doi:Doi 10.1111/J.1365-2486.2008.01673.X, 2008b.

Feng, Z. Z., Niu, J. F., Zhang, W. W., Wang, X. K., Yao, F. F., and Tian, Y.: Effects of ozone exposure on sub-tropical evergreen Cinnamomum camphora seedlings grown in different nitrogen loads, Trees-Structure and Function, 25, 617-625, doi:10.1007/s00468-011-0538-x, 2011a.

Feng, Z. Z., Pang, J., Kobayashi, K., Zhu, J. G., and Ort, D. R.: Differential responses in two varieties of winter wheat to elevated ozone concentration under fully open-air field conditions, Global Change Biology, 17, 580-591, doi:10.1111/j.1365-2486.2010.02184.x, 2011b.

Fu, W., Gao, J., Xu, S., Deng, L., He, X., Chen, W., Zhao, Y., and Su, L.: Effect of high ozone concentration on photosynthesis of Betula platyphylla and Populus alba × P. berolinensi. (in Chinese), Chinese Journal of Ecology, 33, 3184-3190, 2014.

Fu, Y., Zhao, T., Sun, J., Cao, Y., Hu, Y., Xu, L., and Shi, Y.: Effects of Elevated Ozone Concentration on Maize Photosynthesis and Grain Quality (in Chinese), Acta Agriculturae Boreali-Sinica, 23, 120-124, 2008.

Hao, Y., Lin, M., Xue, L., Wang, Z., Lin, J., Liang, Z., Sun, B., and Tian, m.: Effects of ozone stress and drought stress on photosynthesis characteristics of Syzygium hainanense and Alstonia scholaris seedlings (in Chinese), Journal of Anhui Agricultural University, 41, 193-197, 2014.

Hawlader, M. N. A.: Diffuse, global and extraterrestrial solar radiation for Singapore, International Journal of Ambient Energy, 5, 31-38, 1984.
He, X. Y., Fu, S. L., Chen, W., Zhao, T. H., Xu, S., and Tuba, Z.: Changes in effects of ozone exposure on growth, photosynthesis, and respiration of Ginkgo biloba in Shenyang urban area, Photosynthetica, 45, doi:10.1007/s11099-007-0095-0, 2007.
Hoshika, Y., Carriero, G., Feng, Z. Z., Zhang, Y. L., and Paoletti, E.: Determinants of stomatal sluggishness in ozone-exposed deciduous tree species, Sci Total Environ, 481, 453-458, doi:10.1016/j.scitotenv.2014.02.080, 2014.
Karatasou, S., Santamouris, M., and Geros, V.: Analysis of experimental data on diffuse solar radiation in Athens, Greece, for building applications International Journal of Sustainable Energy, 23, 1-11, doi:10.1080/0142591031000148597 2003.
Lam, J. C., and Li, D. H. W.: Correlation between global solar radiation and its direct and diffuse components, Build Environ, 31, 527-535, doi:10.1016/0360-1323(96)00026-1, 1996.
Li, L., Manning, W. J., Tong, L., and Wang, X. K.: Chronic drought stress reduced but not protected Shantung maple (Acer truncatum Bunge) from adverse effects of ozone (O-3) on growth and physiology in the suburb of Beijing, China, Environmental Pollution, 201, 34-41, doi:10.1016/j.envpol.2015.02.023, 2015.
Li, M.: Effects of ozone on photosynthesis of several plants (in Chinese), Environmental Science, 36, 1888-1901, 2015.
Li, Q., Lu, G., Xue, L., Chen, H., Lie, G., Liang, Z., and Sun, B.: Effects of Ozone and Drought Stress on Photosynthetic Physiology of Three Species Seedlings in South China (in Chinese), Guangdong Forestry Science and Technology, 30, 45-52, 2014.
Niu, J. F., Feng, Z. Z., Zhang, W. W., Zhao, P., and Wang, X. K.: Non-Stomatal Limitation to Photosynthesis in Cinnamomum camphora Seedings Exposed to Elevated O-3, Plos One, 9, doi:ARTN e98572
10.1371/journal.pone.0098572, 2014.
Oliveira, A. P., Escobedo, J. F., Machado, A. J., and Soares, J.: Correlation models of diffuse solar-radiation applied to the city of Sao Paulo, Brazil, Appl Energ, 71, 59-73, doi:10.1016/S0306-2619(01)00040-X, 2002.
Orgill, J. F., and Hollands, K. G. T.: Correlation Equation for Hourly Diffuse Radiation on a Horizontal Surface, Sol Energy, 19, 357-359, doi:10.1016/0038-092x(77)90006-8, 1977.
Pang, J., Kobayashi, K., and Zhu, J. G.: Yield and photosynthetic characteristics of flag leaves in Chinese rice (Oryza sativa L.) varieties subjected to free-air release of ozone, Agriculture Ecosystems & Environment, 132, 203-211, 2009.
Reindl, D. T., Beckman, W. A., and Duffie, J. A.: Diffuse Fraction Correlations, Sol Energy, 45, 1-7, doi:10.1016/0038-092x(90)90060-P, 1990.
Soares, J., Oliveira, A. P., Boznar, M. Z., Mlakar, P., Escobedo, J. F., and Machado, A. J.: Modeling hourly diffuse solar radiation in the city of Sao Paulo using a neural-network technique, Appl Energ, 79, 201-214, 2004.
Wang, L. L., He, X. Y., and Chen, W.: Effects of Elevated Ozone on Photosynthetic CO2 Exchange and Chlorophyll a Fluorescence in Leaves of Quercus mongolica Grown in Urban Area, B Environ Contam Tox, 82, 478-481, doi:10.1007/s00128-008-9606-3, 2009.

Xin, Y., Gao, F., and Feng, Z.: Photosynthetic characteristics and ozone dose-response relationships for different genotypes of poplar (in Chinese), Environmental Science, 37, 359-367, 2016.

Xu, S., He, X. Y., Chen, W., Su, D. Y., and Huang, Y. Q.: Elevated CO2 Ameliorated the Adverse Effect of Elevated O-3 in Previous-Year and Current-Year Needles of Pinus tabulaeformis in Urban Area, B Environ Contam Tox, 92, 733-737, doi:10.1007/s00128-014-1246-1, 2014.

Xu, S., He, X., Chen, W., Huang, Y., Zhao, Y., and Li, B.: Differential sensitivity of four urban tree species to elevated O3, Urban Forestry & Urban Greening, 14, 1166-1173, doi:10.1016/j.ufug.2015.10.015, 2015.

Yan, K., Chen, W., He, X., Zhang, G., Xu, S., and Wang, L.: Responses of photosynthesis, lipid peroxidation and antioxidant system in leaves of Quercus mongolica to elevated O3, Environmental and Experimental Botany, 69, 198-204, 2010.

Yuan, X. Y., Calatayud, V., Jiang, L. J., Manning, W. J., Hayes, F., Tian, Y., and Feng, Z. Z.: Assessing the effects of ambient ozone in China on snap bean genotypes by using ethylenediurea (EDU), Environmental Pollution, 205, 199-208, doi:10.1016/j.envpol.2015.05.043, 2015.

Yue, X., and Unger, N.: Fire air pollution reduces global terrestrial productivity, Nat Commun, 9, 5413, doi:10.1038/s41467-018-07921-4, 2018.

Zhang, W., Zhao, T., Wang, M., He, X., and Fu, S.: Effects of elevated ozone concentration on Ginkgo biloba photosynthesis, Chinese Journal of Ecology, 26, 645-649, 2007a.

Zhang, W., Zhao, T., Wang, M., Zhang, X., He, X., and Fu, S.: Effect of Elevated Ozone Concentration on Photosynthesis of Pinus tabulaeformis Carr. (in Chinese), Journal of Agro-Environment Science, 26, 1024-1028, 2007b.

Zhang, W., Niu, J., Feng, Z., Wang, X., Tian, Y., and Yao, F.: Responses of Ilex integra Thunb. Seedlings to Elevated Air Ozone Concentration (in Chinese), Environmental Science, 32, 2414-2421, 2011a.

Zhang, W., Niu, J., Wang, X., Tian, Y., Yao, F., and Feng, Z.: Effects of Elevated Ozone Concentration on Slash Pine (Pinus elliottii) Seedlings (in Chinese), Environmental Science, 32, 1710-1716, 2011b.

Zhang, W., Niu, J., Wang, X., Tian, Y., Yao, F., and Feng, Z.: Effects of ozone exposure on growth and photosynthesis of the seedlings of Liriodendron chinense (Hemsl.) Sarg, a native tree species of subtropical China, Photosynthetica, 49, 29-36, 2011c.

Zhang, W. W., Feng, Z. Z., Wang, X. K., and Niu, J. F.: Responses of native broadleaved woody species to elevated ozone in subtropical China, Environmental Pollution, 163, 149-157, doi:10.1016/j.envpol.2011.12.035, 2012.

Zhang, W. W., Feng, Z. Z., Wang, X. K., and Niu, J. F.: Impacts of elevated ozone on growth and photosynthesis of Metasequoia glyptostroboides Hu et Cheng, Plant Sci, 226, 182-188, doi:10.1016/j.plantsci.2014.06.005, 2014.

Zhao, T., Wang, M., Zhao, Y., Guo, D., He, X., and Fu, S.: Effects of elevated atmospheric ozone concentration on photosynthetic mechanism of Pinus tabulaeformis Carr. (in Chinese), Journal of Beijing Forestry University, 31, 31-36, 2009.

Zheng, Y., Zhang, J., Wu, R., Zhao, Z., and Hu, C.: Effects of ozone stress on photosynthesis and physiological characteristics of winter wheat in northern China, Journal of Agro-Environment Science, 29, 1429-1436, 2010.

Zhuang, M., Chen, S., Li, Y., Guo, Z., Yang, Q., and Deng, Z.: Changes of physiological responses of Phyllostachys edulis to atmospheric ozone stress (in Chinese), Acta Botanica Boreali-Occidentalia Sinica, 33, 132-138, 2013.